Phase behavior and microstructure of symmetric non-ionic microemulsions with long-chain *n*-alkanes and waxes

*Kristina Schneider[a], Tim M. Ott[a], Ralf Schweins[b], Henrich Frielinghaus[c], Oliver Lade[d], Thomas Sottmann[a]**

[a]Institut für Physikalische Chemie, Universität Stuttgart, Pfaffenwaldring 55, 70569 Stuttgart, Germany

[b]Institut Laue-Langevin, 71 avenue des Martyrs, CS 20156, 38042 GRENOBLE Cedex 9, France

[c]Jülich Centre for Neutron Science JCNS at Heinz Maier-Leibnitz Zentrum (MLZ), Lichtenbergstraße 1, 85748 Garching, Germany

[d]Clariant Produkte (Deutschland) GmbH, G 860, Industriepark Höchst, August-Laubenheimer Straße 1, 65929 Frankfurt am Main, Germany

KEYWORDS microemulsions, phase behavior, oil removal, washing process, long-chain *n*-alkanes, technical wax, pure and technical grade surfactants, non-ionic surfactants

ABSTRACT:

Microemulsions are thermodynamically stable, macroscopically isotropic mixtures of at least two immiscible components and a surfactant. Their general features, i.e. the complex phase behavior, the ultra-low interfacial tensions and the multifarious nanostructure, have been systematically elucidated in the last century. However, the efficient solubilization of long-chain *n*-alkanes and waxes, which plays a significant role in enhanced oil recovery, washing, and cosmetics, remains a challenge. Thus, in this work the influence of the *n*-alkane chain length *k* on the phase behavior of ternary (symmetric) microemulsions containing equal volumes of water and oil was studied. Using *n*-alkanes ranging from *n*-dodecane ($C_{12}H_{26}$) to *n*-dotriacontane ($C_{32}H_{66}$) and pure *n*-alkyl polyglycol ether (C_iE_j) surfactants, we found that the efficiency of the respective surfactant decreases linearly with increasing *k*, while the phase inversion temperature (*PIT*) shows a logarithmic dependence. The influence of a technical wax on the phase behavior was studied by means of the systems H_2O □ SASOL*WAX 5805* (Sasol) □ $C_{16}E_6$ yielding an equivalent alkane carbon number (EACN (SASOL*WAX 5805*)) of 30.8. Finally, the pure C_iE_j surfactants were replaced with technical grade counterparts of the Genapol® series (Clariant) finding that the solubilization efficiency of the long-chain Genapol O 080 is comparable to the pure $C_{16}E_6$ surfactant. Using small-angle neutron scattering (SANS) the microstructure of the formulated microemulsions was studied near the so-called optimum ($\tilde{X}$) point. The scattering curves prove, that microemulsions containing long-chain *n*-alkanes and waxes are also bicontinuously structured at the phase inversion temperature (*PIT*). Interestingly, a high degree of structural ordering is found reflected by values of the amphiphilicity factor f_a ranging between -0.83 and -0.87.

1. INTRODUCTION

Microemulsions (ME) are thermodynamically stable, macroscopically homogeneous but nano-structured mixtures consisting of at least three different components, a hydrophilic/polar (A) (e.g. water), a hydrophobic/non-polar (B) (e.g. oil) and an amphiphilic component (C). In general, microemulsions, which in technical applications often contain additional components as e.g. salt, other hydrophilic and hydrophobic components as well as co-surfactants, are stabilized by an extended amphiphilic film. This film separates the two immiscible components, i.e. polar (e.g. H_2O) and nonpolar (e.g. oil), in two domains exhibiting multifarious microstructures.[1–7] Due to their thermodynamic stability, microemulsions are formed spontaneously and offer outstanding properties, which can be adjusted by a series of different parameters as e.g. temperature, salt concentration and co-surfactant/surfactant ratio.[3,8–16] Thus, ultra-low interfacial tensions can be found, when a microemulsion coexists with a water and oil phase.[8,17–22] Furthermore, a variety of microstructures are accessible ranging from spherical to cylindrical droplets to network-like and bicontinuous structures[1,2,4,23]. In the last decades a lot of energy was put into microemulsion research to exploit these favorable properties in a wider range of industrial applications e.g. in synthesis[24,25], pharmaceutics[24–26], cosmetics[24,25], detergents[24,25,27,28], oil recovery processes[24,25,29–32] etc..

R. Schomäcker pursues the idea to exploit the striking features of microemulsions in industrial applications since more than 30 years. Already in his first publication in 1988 he studied together with *B. H. Robinson* and *P. D. I. Fletcher* hydrolysis reactions of enzymes in water-in-oil microemulsions[33]. In 1995 he gave a comprehensive review of the high potential of microemulsions in technical processes[24]. Furthermore *R. Schomäcker* utilized microemulsions for the synthesis of nanocrystalline particles[34] and designed a continuous hydroformylation process utilizing not only the large interfacial area of microemulsions but also their adjustable phase behavior, which allows for the separation of catalyst and product phase[35]. In one of the latest publications, published 2016, microemulsions were utilized for the three step synthesis of the fungicide Boscalid®[36]. So far *R. Schomäcker* published 61 articles on the utilization of microemulsions in industrial applications; they are cited 1225 times.[37]

Beside their application as reaction media, the washing process and the enhanced oil recovery (EOR) are two other important areas of microemulsion application. Both applications deal with the efficient solubilization of mixtures of oil and the wetting/roll-up mechanism, where the ultra-low interfacial tensions at the phase inversion temperature (see below) facilitate the detachment of fat respectively crude oil from the surface[38,39]. While a large number of publications deal with the formulation and characterization of microemulsions containing short and medium chain alkanes[3,40,41], cyclic oils[42], alkyl methacrylates[43], triglycerides[44] and other polar oils[45], to our knowledge only a few studies deal with the solubilization of long-chain *n*-alkanes in microemulsions[40,46]. As the latter articles concentrate only on phase behavior studies of microemulsions containing selected long-chain *n*-alkanes, we took a more comprehensive approach comprising not only the formulation but also the characterization of microemulsions containing long-chain *n*-alkanes and waxes, in order to exploit this class of microemulsions for washing processes and EOR. In more detail, we investigated the influence of the chain length *k* of *n*-alkanes (C_kH_{2k+2}) on the phase behavior and microstructure of symmetric ternary microemulsion systems of the type water – *n*-alkane – non-ionic surfactant increasing the chain length from $k = 12$ (*n*-dodecane, ($C_{12}H_{26}$)) to $k = 32$ (*n*-dotriacontane, ($C_{32}H_{66}$)). With respect to technical application the study was expanded to the technical SASOL*WAX 5805* (Sasol) consisting of a mixture of various long-chain acyclic hydrocarbons/paraffines. The microemulsions were stabilized by pure non-ionic surfactants of the *n*-alkyl polyglycol ether (C_iE_j) type, namely pentaethylene glycol monododecyl ether ($C_{12}E_5$), hexaethylene glycol monotetradecyl ether ($C_{14}E_6$) and hexaethylene glycol monohexyl ether ($C_{16}E_6$) as well as by *Genapol®* surfactants (Clariant). The latter are the much cheaper technical-grade counterparts exhibiting a broad distribution of the ethoxylation degree including a residual amount of unreacted alcohol.

Starting point of this study was the characterization of the phase behavior. $T(\gamma)$-sections through the phase prism were recorded via the determination of the phase boundaries as a

function of temperature and surfactant mass fraction γ at equal volumes of water and oil ($\phi = 0.50$). Main goal was the determination of the so-called optimum-/$\widetilde{X}$-point given by the phase inversion temperature $PIT/\tilde{T}$ and the minimum mass fraction $\tilde{\gamma}$ of surfactant to solubilize water and oil. The great importance of the $\widetilde{X}$-point is reflected by the fact, that the *PIT* marks the temperature where the oil/water interfacial tension σ_{ab} and length scale ξ of the microstructure runs through a minimum and maximum, respectively[47], while the value of $\tilde{\gamma}$ correlates to the absolute values of $\sigma_{ab,min}$ and ξ_{max}[17,48]. In order to study whether the chain length of the *n*-alkane has an influence on the microstructure of symmetric microemulsions, small-angle neutron scattering (SANS) experiments were conducted near the $\widetilde{X}$-point of the respective systems in the one phase region. The experiments were performed adjusting the so-called bulk-contrast, i.e. using D_2O instead of H_2O. Analyzing the SANS-data not only the determination of the periodicity d_{TS} and the correlation length ξ_{TS} of the structure but also the amphiphilicity factor f_a[4,49], which is a measure of the degree of ordering, and the bending rigidity κ of the amphiphilic film[50] can be determined.

2. EXPERIMENTAL SECTION

Materials. We used double-distilled H_2O and the following long-chain *n*-alkanes (C_kH_{2k+2}), with an even number of carbon atoms: *n*-Dodecane ($C_{12}H_{26}$, T_m = -10°C, *Sigma-Aldrich*, purity of >99%), *n*-Hexadecane ($C_{16}H_{34}$, T_m = 18°C, *Sigma-Aldrich*, purity of 99%), *n*-Octadecane ($C_{18}H_{38}$, T_m = 28°C, *Merck*, purity of >99%), *n*-Icosane ($C_{20}H_{42}$, T_m = 37°C, *Acros*, purity of 99%), *n*-Docosane ($C_{22}H_{46}$, T_m = 44°C, *Acros*, purity of 99%), *n*-Tetracosane ($C_{24}H_{50}$, T_m = 51°C, *Acros*, purity of 99%), *n*-Hexacosane ($C_{26}H_{54}$, T_m = 57°C, *Acros*, purity of 99%), *n*-Octacosane ($C_{28}H_{58}$, T_m = 61°C, *Acros*, purity of 99%), *n*-Triacontane ($C_{30}H_{62}$, T_m = 66°C, *Acros*, purity of 98%) and *n*-Dotriacontane ($C_{32}H_{66}$, T_m = 70°C, *Alfa Aesar*, purity of 98%). The technical wax SASOL*WAX 5805* provided by the *Sasol Germany GmbH* consists of a mixture of various long-chain acyclic hydrocarbons/paraffines. The composition of this SASOL*WAX 5805* is specified by the *Sasol*

Germany GmbH via a gas chromatography (GC) spectrum, see the obtained results in the supporting information Figure S1. Based on the recorded GC-spectrum the investigated wax consists of various long-chain linear (*n*) and branched (*iso*) alkanes ranging from C_{19} to C_{46} with an average number of C-atoms amounts to 30.5.

The three pure non-ionic *n*-alkylpolyglycolether surfactants pentaethylene glycol monododecyl ether ($C_{22}H_{46}O_6$, $C_{12}E_5$), hexaethylene glycol monotetradecyl ether ($C_{26}H_{54}O_7$, $C_{14}E_6$) and hexaethylene glycol monohexadecyl ether ($C_{28}H_{58}O_7$, $C_{16}E_6$) were purchased from *Fluka* (Neu Ulm, Germany) with an analytical grade of at least >98%. As technical counterparts, we used the technical-grade C_iE_j's *Genapol LA* and *Genapol O* supplied by *Clariant* (Frankfurt, Germany).

The *Genapol LA* surfactants where synthesized by the ethoxylation of a mixture of alcohols with a mean carbon atom number of C_{12-14}, while the *Genapol O* surfactants are ethoxylated oleyl alcohols. In this work we used *Genapol LA* surfactants exhibiting mean ethoxylation degrees of 4 (*Genapol LA 040*) and 7 (*Genapol LA 070*) as well as *Genapol O* surfactants with a mean ethoxylation degree of 5 (*Genapol O 050*) and 8 (*Genapol O 080*). Note, that these technical-grade surfactants exhibit a broad distribution in the ethoxylation degree.

Examining the microstructure of these symmetric microemulsions by small angle neutron scattering (SANS) H_2O was replaced with D_2O (*Eurisotop*, > 99%) to adjust bulk-contrast. All components are used directly without any further purification. The macroscopic densities ϱ^0 and scattering length densities ϱ calculated with the help of Equation 6 using the scattering length b_i of each component used are listed in Table S1 (Supporting Information).

Methods.

Phase behavior: To obtain the $T(\gamma)$-sections for the respective ternary or pseudo-ternary systems (see schematic drawing of the Gibb's phase prism in Figure 1, left), the samples have to be prepared using certain amounts of surfactants or mixtures of surfactants and equal volumes of

water and oil. Therefore, the samples are weighted into test tubes with an accuracy of $\Delta m = \pm$ 0.001 g in the following order beginning with the nonionic surfactants (C_iE_j). As the used oils (*n*-alkane or wax) are good solvents for the C_iE_i surfactants, they are added to the surfactants in the next step before finally the water is weighed in. After the sample preparation, a stirring bar is added and the test tubes are sealed with a polyethylene stopper. Afterwards the phase diagram of each sample is investigated with the help of a thermostatted water bath (Thermo-Haake DC30 with a temperature control up to $\Delta T = \pm$ 0.01 K). Before starting the investigation of the temperature-dependent phase behavior of the respective systems, all samples have to be homogenized by stirring them at elevated temperatures to ensure that all components in the mixtures are dissolved completely. Then the temperature is controlled to the adjusted temperature under further stirring. When the temperature equilibrium is reached, the stirring process is stopped, and the type and number of coexisting phases are determined visually. To visualize potentially existing liquid anisotropic phases, crossed polarizers are applied additionally. All appearing phases and phase transition temperatures are determined with a precision of $\Delta T = \pm$ 0.05 K. Afterwards the samples are diluted to the next composition.

The sample compositions are given using the nomenclature suggested by *Kahlweit et al.*[3], i.e. the mass fraction α of oil in the water/oil mixture

$$\alpha = \frac{m_B}{m_A + m_B}, \qquad (1)$$

which can be converted into the volume fraction ϕ of oil in the water/oil mixture

$$\phi = \frac{V_B}{V_A + V_B} \qquad (2)$$

using the respective densities. In this study we adjusted the mass fraction α of oil in the water/oil mixture to a value which corresponds to equal volumes of water and oil ($\phi = 0.50$). This

approach is chosen, because it has been shown for these type of systems, that the trajectory of the middle phase microemulsion is symmetric with respect of $\phi = 0.50$[51]. By choosing a microemulsion system symmetric in volumes of water and oil, the amphiphilic film adjusts a zero mean curvature at the phase inversion temperature[1]. Furthermore, Table shows that the value of α is similar for all studied systems, i.e. increases only from $\alpha = 0.430$ in the *n*-dodecane system to $\alpha = 0.449$ in the *n*-dotriacontane system, due to the small differences in the oil density (see Table S1 in the supporting information).

The second parameter to specify the composition of a ternary microemulsion system is the mass fraction of the surfactant (C) in the overall mixture

$$\gamma = \frac{m_C}{m_A + m_B + m_C}. \quad (3)$$

Alternatively, the volume fraction of the surfactant (C) in the overall mixture

$$\phi_C = \frac{V_C}{V_A + V_B + V_C} \quad (4)$$

can be used (see SANS part). If a mixture of two different surfactants is used, the mass fraction of surfactant 2 (C2) in the mixture of surfactant 1 (C1)/surfactant 2 is defined as

$$\delta = \frac{m_{C2}}{m_{C1} + m_{C2}}. \quad (5)$$

Small-angle neutron scattering (SANS): The structural properties of the formulated microemulsions containing long-chain *n*-alkanes are accessed near the optimum ($\widetilde{X}$) point with the help of SANS experiments allowing to adjust different contrasts by varying the hydrogen-deuterium ratio. In this study, we adjusted bulk-contrast by replacing H_2O with D_2O. The

scattering length density difference $\Delta\varrho = \rho_{D_2O} - \rho_{oil}$ between D_2O and oil defines the strength of the contrast. Hereby the scattering length density of a molecule is defined by

$$\rho = \frac{\rho^0 N_A}{M_w} \sum_i b_i, \qquad (6)$$

with N_A being the Avogadro constant, b_i the scattering lengths of atom i, M_w the molar mass and ϱ^0 the macroscopic density of the molecule, respectively. Note, that for varying the contrast, the composition of the microemulsion samples was kept constant with respect to volume fractions. As it is well-known, replacing H_2O with D_2O the phase boundaries of microemulsions stabilized by nonionic surfactants are systematically shifted to lower temperatures by about $\Delta T \approx 2$ K[52].

The scattering experiments were performed at the D11 spectrometer of the *Insitut Laue-Langevin* (ILL) in Grenoble, France and at the KWS-1 spectrometer[53] at the *Heinz Maier-Leibnitz Zentrum* (MLZ) in Munich, Germany. At the D11 spectrometer a neutron wavelength of $\lambda = 4.6$ Å with a wavelength spread of $\Delta\lambda/\lambda = 9\%$ (FWHM), specified by the ILL for the D11 instrument, was used. In order to cover *q*-range from 0.0022 $Å^{-1}$ to 0.5758 $Å^{-1}$, where $q = 4\pi \cdot \sin(\theta/2)/\lambda$ is the absolute value of the scattering vector, we chose the detector/collimation distances 39 m/40.5 m, 8 m/20.5 m and 1.4 m/20.5 m, respectively. At the KWS-1 spectrometer a neutron wavelength of $\lambda = 5.0$ Å with a wavelength spread of $\Delta\lambda/\lambda =$ 10% (FWHM) was used. Adjusting detector/collimation distances 20 m/20 m, 8 m/8 m and 1.5 m/4 m, respectively a *q*-range from 0.0027 $Å^{-1}$ to 0.4030 $Å^{-1}$ was accessible.

The SANS samples were filled in Hellma quartz QS glass cells (optical path length of 1 mm) which are rapidly transferred to a homebuilt cell holder (ILL) respectively a similar four position cell holder provided by the Jülich Center for Neutron Research (JCNS) which allowed adjusting the temperature to ±0.1 K. Furthermore, both cell holders can be shaken manually to ensure the homogenization of the respective sample[54,55]. By checking each sample before and after the

measurement via visual inspection, it is ensured that the samples have been in the homogeneous one-phase state during the measurements.

The scattering intensity was normalized to absolute scale using the incoherent scattering of H_2O and perspex (optical path length of both: 1 mm) as reference. The raw data treatment, masking and radial averaging to obtain a one dimensional scattering spectrum was performed using the evaluation software packages *LAMP* and *QtiKWS* provided by the ILL and JCNS, respectively. Background correction and the detector dead time are included to obtain the differential cross section $d\sigma(q)/d\Omega=I(q)$.

GENERAL BACKGROUND INFORMATION

Phase behavior of ternary microemulsion systems: For most applications of microemulsion systems, it is important to gain knowledge on their properties such as the oil/water interfacial tension σ_{ab} or the length scale ξ of the microstructure. Thus, at the beginning of a study, the phase behavior has to be investigated. Restricting ourselves to ternary systems consisting of water, oil and an amphiphilic component at constant pressure, the temperature dependent phase behavior is most appropriately illustrated in an upright Gibbs phase prism (Figure 1, left). Since it is very time-consuming to investigate the phase behavior over the whole temperature and composition ranges, it has been proven useful to perform some vertical sections through the phase prism[3].

In this work $T(\gamma)$-sections, i.e. the so-called "fish"-sections, are recorded, as they are the method of choice to determine the optimum-/$\tilde{X}$-point at which not only the surfactant solubilizes the maximum amounts water and oil (minimum mass fraction of surfactant $\tilde{\gamma}$ at the phase inversion temperature $PIT/\tilde{T}$), but also the oil/water interfacial tension σ_{ab} and the length scale ξ of the microstructure runs through a minimum and maximum, respectively. In $T(\gamma)$-sections the phase boundaries are determined as a function of temperature T and surfactant mass fraction γ at

a constant oil-to-water ratio ϕ (for our studies $\phi = 0.50$). In Figure 1, left such a $T(\gamma)$-section is schematically shown inside the Gibbs phase prism. It illustrates the typical "fish"-like shape of the phase boundaries together with the most important parameters and the characteristic phase sequence for non-ionic microemulsion systems. In the following, the main features of this phase diagram are described.

At very low surfactant mass fractions $\gamma < \gamma_0$, a two-phase region can be found over the entire temperature range. In this regime, the macroscopic interface between the coexisting water and oil phase is partially saturated by surfactant molecules and in addition, the surfactant molecules are monomerically dissolved within the water and the oil phase. Increasing the mass fraction of surfactant to $\gamma_0 < \gamma < \tilde{\gamma}$ a three-phase region, denoted by 3, appears at intermediate temperatures. Within this region a surfactant-rich microemulsion (middle) phase coexists with both a lower excess water phase and an upper excess oil phase. Note, that the two excess phases contain monomerically dissolved surfactant molecules. Temperature-wise this three-phase region is limited by the lower and upper critical endpoint temperature T_l and T_u. At temperatures below T_l, an oil-in-water (o/w) microemulsion coexists with an oil excess phase (denoted as $\underline{2}$), whereas at $T > T_u$ a water-in-oil (w/o) microemulsion coexists with a water excess phase (denoted as $\overline{2}$). Thus, the phase sequence of $\underline{2} \square 3 \square \overline{2}$ is found with increasing T at intermediate surfactant mass fractions, which is one feature of microemulsion systems stabilized by nonionic surfactants.

By increasing γ further, a one phase microemulsion (denoted as 1) is obtained at the surfactant mass fraction $\tilde{\gamma}$ and the phase inversion temperature $\tilde{T}$. At this temperature the system is in the so-called balanced state, i.e. the surfactant film possesses a mean curvature of zero by forming a bicontinuous structure[1]. $\tilde{\gamma}$ specifies the minimum mass fraction of surfactant that is needed to solubilize the two immiscible components, here water and oil, completely in one (bicontinuous) phase. Thus, $\tilde{\gamma}$ can be considered as a measure of the solubilization efficiency of the used

surfactant or surfactant mixture. $\tilde{T}$ and $\tilde{\gamma}$ define the optimum-/ $\tilde{X}$-point of a microemulsion system at a given oil-to-water ratio. At $\gamma > \tilde{\gamma}$ the phase sequence $\underline{2} \square 1 \square \overline{2}$ is found as a function of temperature. For typical non-ionic microemulsions, a liquid crystalline phase L_α, which is surrounded by a two-phase region consisting of a microemulsion (ME) and a L_α-phase, can be observed at larger γ-values. Such a behavior is found for the microemulsion systems studied in this work.

Figure 1.

In industrial applications, technical-grade surfactants are used instead of the very expensive pure surfactants. Common non-ionic technical-grade surfactants are ethoxylated alcohols or ethoxylated alkyl phenols. Technical-grade surfactants have a broad distribution of the ethoxylation degree and a residual amount of non-reacted alcohol, but can be treated as a single (pseudo) component. Thus, the phase behavior of such a pseudo-ternary system can also be characterized by $T(\gamma)$-sections[40]. However, the "fish" becomes differently shaped, i.e. the "fish body" is tilted to higher temperatures (Figure 1, right). This is a consequence of the different monomeric solubilities of the differently ethoxylated surfactant homologues. Ethoxylated alcohols are solubilized monomerically in the oil much more than in the water[56]. Surfactant homologues with a lower degree of ethoxylation, i.e. the more hydrophobic species, are more soluble in oil than the ones with a higher degree of ethoxylation, i.e. the more hydrophilic species. Diluting a microemulsion with water and oil, especially the hydrophobic surfactant homologues are dissolved both in the oil-rich domains of the microemulsion and the oil excess phase – leaving the remaining surfactant mixture in the amphiphilic film more hydrophilic. As a consequence the phase boundaries shift to increasingly higher temperatures upon dilution causing the strong distortion of the three phase body towards higher temperatures. Note, that for

the same reason also the temperature of the balanced state, i.e. the *PIT*, depends on γ in microemulsion systems stabilized by technical-grade surfactants, or being more general surfactant mixtures.

Correlation between phase behavior of microemulsion systems and successful oil-removal in washing processes: Former studies on microemulsion systems showed that there is a strong correlation between the phase behavior, the related interfacial tensions and the removal of oil during washing processes[27,28,57]. The removal of oil during washing and cleaning processes and the displacement of oil from narrow capillaries, as it is the case in the enhanced oil recovery (EOR), demand for an as low as possible oil/water-interfacial tension to obtain an optimal soil removal[30]. In microemulsion systems consisting of e.g. water, oil and surfactant, the oil/water-interfacial tension becomes very low when the three-phase region is traversed. Thus, the best washing efficiencies should be observed in the three-phase region of the respective formulation. To proof this correlation, "expensive" washing tests were performed at different temperatures using aqueous solutions of the pure surfactants $C_{12}E_4$ and $C_{12}E_5$ to clean fabrics contaminated with *n*-hexadecane[27,57]. On the right-hand side of Figure 2, the washing temperature is plotted versus the washing efficiency specified by the reflectance *R* determined by photometric measurements. As can be seen, the maximum of oil removal is obtained at $T \approx 30°C$ and $T \approx 50°C$ using the aqueous $C_{12}E_4$ and $C_{12}E_5$-solution, respectively. By comparing these results with the temperature intervals (T_u - T_l) of the three phase body shown on the left-hand side of Figure 2 for a series of microemulsion systems water – *n*-alkane (C_kH_{2k+2}) – $C_{12}E_4$ and $C_{12}E_5$[3,27,57], it becomes obvious, that the highest washing efficiency is gained, where the respective water – *n*-hexadecane (C_kH_{2k+2}) – $C_{12}E_4$ and $C_{12}E_5$ system exhibits its three phase region. Thus, these results prove, that the very low interfacial tensions occurring in the three-phase region of microemulsion systems are the trigger for high washing efficiencies.

Figure 2.

Scattering theory: As discussed before, another outstanding property of microemulsions is their multifarious microstructure. Therefore, we studied also the microstructure of nonionic microemulsions containing long-chain *n*-alkanes near the respective optimal point ($\widetilde{X}$) via SANS (see Figure 1). Former studies have shown that near the $\widetilde{X}$-point the microemulsion consists of water- and oil-rich domains, separated by a connected randomly oriented monolayer of surfactant molecules[58–60]. *Teubner* and *Strey*[49] could show, that bulk-contrast SANS curves of bicontinuously-structured microemulsions can be described by

$$I(q) = \frac{1}{a_2 + c_1 q^2 + c_2 q^4} + I_{\text{incoh.}}, \tag{7}$$

where a_2, c_1 and c_2 are the coefficients of the order parameter expansion defining the periodicity d_{TS}, the correlation length ξ_{TS} and the amphiphilicity factor f_a[4,49,55] according to

$$f_a = \frac{a_1}{\sqrt{4 a_2 c_2}}, \tag{8}$$

$$d_{TS} = 2\pi \left[\frac{1}{2} \left(\frac{a_2}{c_2} \right)^{1/2} - \frac{1}{4} \frac{c_1}{c_2} \right]^{-1/2} \text{ and} \tag{9}$$

$$\xi_{TS} = \left[\frac{1}{2} \left(\frac{a_2}{c_2} \right)^{1/2} + \frac{1}{4} \frac{c_1}{c_2} \right]^{-1/2}. \tag{10}$$

However, a more convenient fitting of the scattering data by the *Teubner-Strey* model can be obtained using the scattering intensity I_0 extrapolated to $q = 0$ values, the intensity $I_{\max}$ and position $q_{\max}$ of the scattering peak and the intensity of the incoherent background $I_{\text{incoh.}}$ using the following equation

$$I(q)=\frac{I_0}{\left(1-\frac{I_0}{I_{\max}}\right)\left(\frac{q^2}{q_{\max}^2}-1\right)^2+\frac{I_0}{I_{\max}}}+I_{\text{incoh.}}. \tag{11}$$

Another important parameter which can be extracted from the analysis of the scattering peak by the *Teubner-Strey* model is the renormalized bending rigidity κ_{SANS} of the amphiphilic film. The bending rigidity is one important parameter in the bending free energy introduced by *Helfrich*[61], which has been successfully used to describe the properties of microemulsion systems[50,62–65]. According to *Safran et al.*[63] κ_{SANS} can be obtained by using the model of random interfaces according to

$$\frac{\kappa_{\text{SANS}}}{k_{\text{B}}T}=\frac{10\sqrt{3}\pi}{64}\frac{\xi_{\text{TS}}}{d_{\text{TS}}}, \tag{12}$$

with k_{B} and T being the *Boltzmann* constant and temperature, respectively.

While the *Teubner-Strey* model was used to analyze the scattering peak, the large q-part of the scattering curve was described by *Porod*'s decay for diffuse interfaces (Equation 13). Following *Strey et al.*[66] the diffuseness of the amphiphilic film can be taken into account by the convolution of the step profile of a sharp interface with a smooth Gaussian profile of standard deviation t according to

$$\lim_{q\to\infty}[I(q)]=2\pi\langle\Delta\rho^2\rangle\frac{S}{V}q^{-4}\exp(-q^2t^2)+I_{\text{incoh.}}, \tag{13}$$

with $\Delta\varrho$ being the difference of the scattering length densities of the water and oil domains and S/V the area of the specific internal interface. By using the so-called scattering invariant Q_{i}

$$Q_{\text{i}}=\int_0^\infty q^2I(q)dq=2\pi^2\phi_{\text{a}}\phi_{\text{b}}\langle\Delta\rho^2\rangle \tag{14}$$

introduced by *Porod et. al*[67], the specific internal interface S/V can be determined by

$$\frac{S}{V} = \frac{\pi \phi_a \phi_b \, q^4 \exp(q^2 t^2)}{Q_i} \cdot \left(\lim_{q \to \infty} [I(q)] - I_{\text{incoh.}} \right). \quad (15)$$

This new approach makes it possible to eliminate inaccuracies of the absolute calibration of the intensity $I(q)$, which is excluded in Equation 13. By knowing the specific internal interface S/V, the molecular volume v_c and the head group area a_c (calculated from[52]) of the respective surfactant, the volume fraction of surfactant in the interface $\Phi_{c,i}$ can be calculated utilizing

$$\phi_{c,i} = \frac{S}{V} \frac{v_c}{a_c} \quad (16)$$

and hence the volume fraction $\Phi_{mon,b}$ of surfactant molecules solubilized within the oil-phase of the respective microemulsion (see[56] for further details).

3. RESULTS AND DISCUSSION

Phase behavior of microemulsions of the type water – long-chain *n*-alkanes – pure *n*-alkyl polyglycol ether (C_iE_j) surfactants

As mentioned in the introduction, the solubilization of long-chain *n*-alkanes and waxes plays a significant role in technical applications, as e.g. the washing process and EOR. Also from a fundamental research perspective it is of interest whether the decreasing penetration ability of long-chain *n*-alkanes leads to not only a decreasing efficiency of the surfactants to solubilize these oils but also a decreasing degree of microstructural ordering. As to our knowledge only a few studies deal with the solubilization of only selected long-chain *n*-alkanes in microemulsions[40,46], we investigated the influence of the chain length k of *n*-alkanes (C_kH_{2k+2}) on the phase behavior and microstructure of symmetric ternary microemulsion systems of the type

water – *n*-alkane – non-ionic surfactant increasing the chain length from $k = 12$ (*n*-dodecane, ($C_{12}H_{26}$)) to $k = 32$ (*n*-dotriacontane, ($C_{32}H_{66}$)) in steps of two.

The recorded $T(\gamma)$-sections are shown in Figure 3. Being mainly interested in the determination of the optimum/$\tilde{X}$-point, the phase boundaries were only determined for surfactant mass fraction larger than $\tilde{\gamma}$. As can be seen, all phase diagrams exhibit the typical features of microemulsion systems stabilized by pure non-ionic surfactants (see General Background Information), i.e. a $\underline{2} \square 1 \square \bar{2}$ sequence with increasing temperature. Using long-chain surfactants, in most systems a lamellar (L_α)-phase was observed at larger values of γ, surrounded by a regime, where microemulsion and L_α-phase coexist. Furthermore, the following general trends can be observed: increasing the chain length k of the *n*-alkane, the phase boundaries shift to higher temperatures, which can be traced back to the increasing lower miscibility gap of the binary *n*-alkane/C_iE_j system. At the same time the respective surfactant becomes less efficient, which might be related to the higher temperature leading to a less ordered amphihilic film and the fact, that increasing the chain length of an *n*-alkane, it is less able to penetrate into the amphiphilic film. Note, that the $\tilde{X}$-points, i.e. the values of $\tilde{\gamma}$ and $\tilde{T}$ of all studied systems are compiled in Table 1.

In the following the results are discussed in more detail starting with Figure 3A), which shows the $T(\gamma)$-sections of the $C_{12}E_5$-systems. As can be seen, the $\tilde{X}$-point shifts from $\tilde{\gamma} = 0.154$ to $\tilde{\gamma} = 0.230$ using *n*-icosane ($C_{20}H_{42}$) instead of *n*-hexadecane ($C_{16}H_{34}$). Having in mind the solubilization of really long-chain *n*-alkanes we, at this point, replaced the surfactant $C_{12}E_5$ with $C_{14}E_6$ (Figure 3B)). Comparing the efficiency of these two surfactants in solubilizing *n*-icosane, it becomes obvious that $\tilde{\gamma}$ is reduced to $\tilde{\gamma} = 0.154$ utilizing $C_{14}E_6$. This effect of the surfactant alkyl length on the efficiency is well known (e.g.[56]) and can be related to an increasing bending rigidity κ. Theory predict that $\kappa \sim l^3$, with l being the length of the hydrophobic part of the surfactant.

Using the surfactant $C_{14}E_6$, *n*-alkanes ranging from *n*-dodecane ($C_{12}H_{26}$) to *n*-octacosane ($C_{28}H_{58}$) are solubilized (Figure 3B)), observing an increase of the $\widetilde{X}$-point to $\tilde{\gamma} = 0.286$ and to $\tilde{T} = 78.3$ for the *n*-octacosane system. Finally in order to decrease $\tilde{T}$ (i.e. the *PIT*) and to increase the efficiency, the surfactant $C_{14}E_6$ was replaced with $C_{16}E_6$ (Figure 3C)). Comparing the $\widetilde{X}$-points of the two *n*-octacosane systems, a strong decrease to $\tilde{\gamma} = 0.146$ and $\tilde{T} = 66.7$°C is found when the surfactant $C_{16}E_6$ is used. As can be seen in Figure 3C), increasing the chain length of the *n*-alkane to $k = 32$ (*n*-dotriacontane), the $\widetilde{X}$-point shifts to $\tilde{\gamma} = 0.195$ and $\tilde{T} = 66.7$°C.

Figure 3.

Table 1.

In the following, the variation of the optimum/$\widetilde{X}$-point with the oil chain length *k* is discussed by plotting the "adapted" surfactant mass fraction $\tilde{\gamma} + \Delta\tilde{\gamma}$ (Figure 4) and phase inversion temperature $\tilde{T} + \Delta\tilde{T}$ (Figure 5) as a function of *k*. In order to compare the $\tilde{\gamma}$ and $\tilde{T}$ values of microemulsion systems stabilized by different surfactants, the values of the $C_{12}E_5$-systems are shifted by $\Delta\tilde{\gamma}[C_{12}E_5] = -0.0650$ and $\Delta\tilde{T}[C_{12}E_5] = 6.0$ K, while the values of the $C_{16}E_6$-systems are altered by $\Delta\tilde{\gamma}[C_{16}E_6] = 0.1400$ and $\Delta\tilde{T}[C_{16}E_6] = 11.5$ K using the $C_{14}E_6$-system as standard system ($\Delta\tilde{\gamma}[C_{14}E_6] = 0$ and $\Delta\tilde{T}[C_{14}E_6] = 0$ K). The $\Delta\tilde{\gamma}$ and $\Delta\tilde{T}$ values are determined comparing the $\widetilde{X}$-points of the systems H_2O – *n*-icosane – $C_{12}E_5$ and $C_{14}E_6$ as well as the $\widetilde{X}$-points of the systems H_2O – *n*-octacosane – $C_{14}E_6$ and $C_{16}E_6$. Furthermore, in order to extend this representation to nonionic microemulsion containing intermediate chain *n*-alkanes, values of the $\widetilde{X}$-points of $C_{12}E_5$-systems with *n*-octane, *n*-decane, *n*-dodecane and *n*-tetradecane are taken from[56].

As can be seen in Figure 4, the "adapted" surfactant mass fraction $\tilde{\gamma} + \Delta\tilde{\gamma}$ depends linearly on the chain length k of the *n*-alkanes. Thus, the surfactant mass fraction at the $\widetilde{X}$-points of microemulsion systems stabilized by the C_iE_j-surfactants and containing any *n*-alkane ($4 < k < 40$) can be predicted using

$$\tilde{\gamma} = 0.0154\ k - 0.1506 - \Delta\tilde{\gamma}\ . \qquad (17)$$

While the $\Delta\tilde{\gamma}$-values of the $C_{12}E_5$ and $C_{16}E_6$-systems are determined in this work (using the $C_{14}E_6$-systems as standard system), the $\Delta\tilde{\gamma}$-values of microemulsion systems stabilized by other C_iE_j surfactants can be determined using literature data[56].

Figure 4.

Interestingly, plotting the "adapted" phase inversion temperature $\tilde{T} + \Delta\tilde{T}$ versus the chain length k of the *n*-alkanes no linear trend is observed. Thus, by extending these studies over such a wide range of *n*-alkanes, we were for the first time able to show that the *PIT* depends rather logarithmically on k than linearly, as it is claimed in literature[40,46] where the $T(\gamma)$-section is recorded at $\alpha = 0.5$. Note, that examining Figure 10 (top) of reference[40] more closely, a non-linear behavior of the phase inversion temperature is already visible in their results. The phase inversion temperature of microemulsion systems stabilized by the C_iE_j-surfactants and containing any *n*-alkane ($4 < k < 40$) can be predicted using

$$\tilde{T} = 32.3\ \ln(k) - 30.1\ °C - \Delta\tilde{T} \qquad (18)$$

Note, that while the $\Delta\tilde{T}$-values of the $C_{12}E_5$ and $C_{16}E_6$-systems are determined in this work (using the $C_{14}E_6$-systems as standard system), the $\Delta\tilde{T}$-values of microemulsion systems stabilized by other C_iE_j surfactants can be determined using literature data[56].

Figure 5.

Solubilization of technical-grade oils in microemulsions stabilized by pure C_iE_j-surfactants

With the aim to extend the studies to more technically relevant microemulsion systems, which was already an early motive in *R. Schomäcker's* work in the 1990s, we studied the solubilization of a technical-grade oil in the next step. As technical oil we used the wax SASOL*WAX 5805*, which is a mixture of various long-chain linear (*n*-) and branched (*iso*-) alkanes, ranging from C_{19} to C_{46}, resulting in an average number of 30.5 C-atoms according to the GC-spectrum.

As the SASOL*WAX 5805* contains rather long-chain oil components we utilized the long-chain surfactant $C_{16}E_6$ to formulate a microemulsion. Figure 6 shows the $T(\gamma)$-section of the system water – SASOL*WAX 5805* – $C_{16}E_6$ recorded at $\square = 0.50$. As can be seen, the SASOL*WAX 5805* can be solubilized in form of a microemulsion, showing the typical features of microemulsion phase behavior. The respective $T(\gamma)$-section of the system water – *n*-octacosane – $C_{16}E_6$ is shown for comparison. Replacing the pure *n*-alkane *n*-octacosane by the SASOL*WAX 5805* the phase boundaries of the SASOL*WAX 5805* containing system are shifted to slightly higher temperatures and higher γ-values. However, the extension of the two-phase coexistence of microemulsion and L_α-phase remains the same, indicating that the SASOL*WAX 5805* stabilizes the L_α-phase. Note, that the values of the $\tilde{X}$-point are included in Table 1.

Using the equivalent alkane carbon number (EACN) concept, both the $\tilde{\gamma}$ and $\tilde{T}$ value of the microemulsion with the SASOL*WAX 5805* is correlated with the $\tilde{X}$-points of the

microemulsions containing the pure *n*-alkanes. As can be seen in Figure 4 and Figure 5, the EACN value of the SASOL*WAX 5805* amounts to EACN ≈ 30.8, which is in good agreement with the average number of 30.5 C-atoms obtained from the GC-spectrum (see Figure S1 in the supporting information).

Figure 6.

Technical-grade alcohol ethoxylates (C_iE_j) for the formulation of microemulsions containing the long-chain *n*-alkane *n*-octacosane

In a next step towards the utilization of microemulsions containing long-chain *n*-alkanes in industrial applications, the very expensive pure C_iE_j surfactants are replaced by their technical-grade counterparts, i.e. surfactants of the *Genapol*® series. The long-chain *n*-alkane *n*-octacosane is chosen to compare the solubilization efficiency of the *Genapol*®-surfactants with the pure surfactant $C_{16}E_6$. In Figure 7 the $T(\gamma)$-sections of the respective microemulsion systems recorded at $\square = 0.50$ are shown. In a first step $C_{16}E_6$ was replaced with a mixture of *Genapol LA 040*/ *Genapol LA 070* ($\delta = 0.50$) made from alcohols with a mean carbon atom number of $C_{12\text{-}14}$. As can be seen, the phase boundaries are shifted to higher temperatures and much higher γ-values. Thus, the LA 040/LA 070-mixture is much less efficient in solubilizing *n*-octacosane than $C_{16}E_6$, which is a consequence of the shorter alkyl length *i* of the surfactant. In order to increase the efficiency, 50 wt% of the *LA 040*/ *LA 070*-mixture is replaced with *Genapol O 080*, which possesses a longer aklyl chain of C_{18}. As a consequence, the phase boundaries shift to lower surfactant mass fractions, but also slightly higher temperatures, which is caused by the high ethoxylation degree of the *Genapol O 080* (~ 8 ethoxy units). In a last step, the remaining *LA 040*/ *LA 070*-mixture is replace with the hydrophobic *Genapol O 050*. As can be seen, using the *Genapol O 050*/*Genapol O 080* ($\delta = 0.50$) mixture, the phase boundaries shift to both lower surfactant mass fractions and lower temperatures. In comparison to the pure surfactant $C_{16}E_6$ the technical-grade *Genapol O*

050/O 080 mixture solubilizes *n*-octacosane slightly more efficient at a higher phase inversion temperature. In conclusion, we are able to show, that long-chain technical-grade alcohol ethoxylates can be successfully used for the formulation of application-related microemulsions containing long-chain *n*-alkanes. Note, that the values of the $\tilde{X}$-points are included Table 1.

Microstructure of symmetric microemulsions with long-chain *n*-alkanes and waxes studied by SANS

In order to study the influence of the chain length of *n*-alkanes (C_kH_{2k+2}) on the microstructure of symmetric (ϕ=0.50) microemulsions of the type water – *n*-alkane – C_iE_j, SANS measurements are performed in the so-called bulk-contrast, i.e. by replacing H_2O by D_2O. All samples are examined near the $\tilde{X}$-point of the respective system (Table 2). In order to perform the measurements, the microemulsion under study has to be stable over a temperature interval of at least 0.3 K. Thus, the microstructure of the microemulsions is studied not exactly at the $\tilde{X}$-point, but at a slightly larger surfactant mass fraction of the order of $\gamma \approx \tilde{\gamma} + 0.01$.

On the left side of Figure 8 the scattering curves of selected symmetric microemulsions of the type water – *n*-alkane – pure C_iE_j are shown by plotting the absolute scattering intensity I (after subtraction of the incoherent background scattering intensity I_{incoh}) as a function of the scattering vector q in a double-log plot. On the right-hand side of Figure 8 the scattering curves of the microemulsions containing either the technical-grade oil or surfactants, namely D_2O – *n*-octacosane – *Genapol O 050/080* and D_2O – SASOL*WAX 5805* – $C_{16}E_6$, are plotted together with the curve of the water – *n*-octacosane – $C_{16}E_6$ microemulsion. Note, that the curves in both plots

are displaced by factors of 10, while the D_2O – *n*-hexadecane – $C_{12}E_5$ data (Figure 8, left) and the D_2O – *n*-octacosane – $C_{16}E_6$ data (Figure 8, right) are shown on absolute scale, respectively.

Figure 8.

All recorded SANS curves show the same two predominant features of bicontinuously structured microemulsions. Namely a scattering peak at intermediate *q*-values and an $exp(-q^2 t^2)q^{-4}$ decay of the scattering intensity at large *q*-values. While the former points towards an ordered structure with a well-defined periodicity, the latter indicates towards the existence of internal interfaces leading to a change of the scattering length density from D_2O-rich to protonated oil-rich domains[68]. Comparing the scattering curves of the D_2O – *n*-alkane – C_iE_j microemulsions (Figure 8, left), the following general trends can be observed: increasing the chain length of the *n*-alkane (using the same surfactant), the scattering peak is shifted to higher *q*-values, as expected from the larger surfactant mass fraction needed to form a bicontinuous microemulsion. Interestingly, the shape of the scattering peak is similar for all studied systems although the *n*-alkane chain length is increased from *n*-hexadecane to *n*-dotriacontane. However, one has to keep in mind that the alkyl chain length of the surfactant is increased at the same time from $C_{12}E_5$ (blue symbols) over $C_{14}E_6$ (green symbols) to $C_{16}E_6$ (pink symbols). By using a surfactant with a longer alkyl chain, the efficiency to formulate a microemulsion with a given oil is increased (see Figure 3), which leads to a shift of the scattering peak to lower *q*-values. Comparing the scatttering curves of the microemulsion containing the SASOL*WAX 5805* (squares), one stabilized by the technical-grade surfactant mixture *Genapol O 050/080* and one stabilized by the pure $C_{16}E_6$ surfactant, the following trends are observed: Solubilizing the SASOL*WAX 5805* instead of *n*-octacosane the peak is shifted to higher *q*-values and is less pronounced, as expected

from the larger surfactant mass fraction needed to form the SASOL*WAX 5805* microemulsion. Interestingly, replacing the $C_{16}E_6$ with the *Genapol O 050/080* mixture, a shift of the peak to lower *q*-values is observed, which seems to be stronger than expected from the only slightly lower surfactant mass fraction.

The scattering data are analyzed using the *Teubner-Strey* (*TS*) model (see Equations 7 and 11) to fit the region of the scattering peak. As can be seen, the *TS*-model (solid lines) describe the scattering peak almost quantitatively yielding the periodicity d_{TS}, correlation lengths ξ_{TS}, amphiphilicity factor f_a and renormalized bending rigidity κ_{SANS}. The results obtained from the *TS*-fits are summarized in Table 2. What immediately strikes the eye are the strongly negative values of the amphiphilicity factor f_a varying between -0.83 and -0.86 indicating the presence of well-structured bicontinuous microemulsions[4,55,69]. For a given surfactant, the periodicity d_{TS} and accordingly the size $d_{TS}/2$ of the water-/oil-rich domains in the bicontinuous structure decrease with increasing oil chain length *k*. The same effect was already found by *Schubert* et al.[4] and *Sottmann* et al.[52] for microemulsions containing *n*-alkanes with shorter chain length and can be related to at least two effects: Firstly, increasing the chain length of an *n*-alkane, it is less able to penetrate into the amphiphilic film, which not only increases its curvature but also decreases its bending rigidity. Secondly, due to the effect on the curvature, the phase boundaries are shifted to higher temperature leading to a less ordered film and thus also to a lower value of the renormalized bending rigidity κ_{SANS}, as can be seen in Table 2. This trend goes hand in hand with a slightly less negative value of the amphiphilicity factor indicating a slightly less ordered structure.

Table 2.

The large *q* part of the scattering curves is analyzed using *Porod*'s decay for diffuse interfaces ($q^{-4}\ exp(-q^2\ t^2)$, Equation 13)[66]. As can be seen in Figure 8 the fits, shown as black dashed lines,

describe the large *q*-part of the scattering curves quantitatively. Using the so-called scattering invariant Q_t, the specific internal interface *S*/*V* can be directly determined from the scattering intensity at $qt > 0.2$ (Equation 15). Only two fit parameters are needed: the diffuseness of the amphiphilic film *t* and the incoherent background $I_{\mathrm{incoh.}}$, which can be read-off from the scattering curve. As the specific internal interface *S*/*V* is proportional to the volume fraction of the surfactant in the interface $\Phi_{s,i}$ (Equation 16), $\Phi_{s,i}$ and the volume fraction $\Phi_{mon,b}$ of surfactant dissolved monomerically within the oil-domains of the microemulsion can be determined[56].

The results obtained from the analysis of the large *q*-part of the scattering curve, which are summarized in Table 2, provide similar conclusions than the analysis of the scattering peak by the *Teubner-Strey*-model. Increasing the chain length of the *n*-alkane (using the same surfactant), the values of specific internal interface *S*/*V* and the volume fraction of the surfactant in the interface $\Phi_{s,i}$ are shifted to higher values, as expected from the larger surfactant mass fraction needed to form a bicontinuous microemulsion. The *n*-octacosane microemulsion stabilized by the *Genapol O 050/080* mixture exhibits the lowest values of $S/V = 0.009$ Å^{-1} and $\Phi_{s,i} = 0.124$, which correlates very well with largest periodicity $d_{TS} = 478$ Å of the bicontinuous microstructure. The monomeric solubility $\Phi_{mon,b}$ of surfactant in the oil-domains decreases slightly with the alkyl length *i* of the surfactant and can be related to its increasing amphiphilicity, which increases the tendency to reside in the amphiphilic film[56].

4. CONCLUSION

The large variety of applications as well as the steadily increasing number of papers and patents on microemulsions show their significance for many branches of chemistry and suggests that microemulsions will become even more significant in the future. In continuing on this road, which is also pursued by *R. Schomäcker*, we studied the properties of microemulsions containing long-chain *n*-alkanes and waxes as attractive candidates for technical applications, as e.g.

washing and EOR processes. In a first set of experiments we investigated the influence of the chain length k of long-chain *n*-alkanes (C_kH_{2k+2}) on the phase behavior of ternary microemulsion containing equal volumes of water and oil. Using the pure non-ionic *n*-alkyl polyglycol ether type surfactants $C_{12}E_5$, $C_{14}E_6$ and $C_{16}E_6$, the chain lengths of the *n*-alkanes were varied from *n*-dodecane ($C_{12}H_{26}$) to *n*-dotriacontane ($C_{32}H_{66}$). The main result of this part of the study is the trend of the so-called optimum microemulsion formed at the $\tilde{X}$-points with the oil chain length k. While the minimum mass fraction $\tilde{\gamma}$ of the surfactant needed to formulate a symmetric microemulsion shows the well-known linear increase, we found for the first time, that the phase inversion temperature (*PIT*/$\tilde{T}$) increases logarithmically with k. Extending our studies to the solubilization of the technical-grade SASOL*WAX 5805* consisting of a mixture of many various long-chain acyclic hydrocarbons/paraffines an equivalent alkane carbon number of EACN ≈ 30.8 (which is in good agreement with the average number of 30.5 C-atoms obtained from the GC-spectrum) could be determined correlating the *PIT* of this technical relevant microemulsion with the $\tilde{T}(k)$-dependence found for *n*-alkane microemulsions. In a next step towards industrial applications the expensive pure C_iE_j surfactants were replaced by their cheap technical-grade counterparts, i.e. surfactants of the Genapol® series. We found, that the efficiency to solubilize the long-chain *n*-alkane *n*-octacosane can be increased, when the technical-grade *Genapol O 050/O 080* mixture is used instead of the pure $C_{16}E_6$ surfactant. In the second part of this paper, the microstructure of these microemulsions is studied by SANS measurements adjusting the so-called bulk-contrast, i.e. by replacing H_2O by D_2O. We found, that the recorded scattering curves show the typical features of bicontinuously structured microemulsions. Interestingly, the curves exhibit a pronounced scattering peak indicating a high degree of structural ordering, although long-chain *n*-alkanes and waxes are solubilized. Analyzing the scattering data with the *Teubner-Strey* model the periodicity d_{TS} of the microstructure, its correlation lengths ξ_{TS}, the amphiphilicity factor f_a and the renormalized bending rigidity κ_{SANS} could be determined. Thereby, it turned out, that the *n*-octacosane

microemulsion stabilized by the *Genapol O 050/080* mixture exhibits the largest periodicity d_{TS} = 478 Å, which correlates well with the lowest specific internal interface S/V = 0.009 Å^{-1} = 9000 m^2/cm^3 and the lowest volume fraction of the surfactant in the interface Φ_{cd} = 0.124.

Supporting information

Table S1. Macroscopic densities ϱ^{0} and scattering length densities ϱ of the components of the investigated ternary microemulsion samples.

Figure S1. Distribution of linear and branched alkanes as a function of their number of C-atoms obtained from a gas chromatography (GC) spectrum of the SASOL*WAX 5805* recorded by the *Sasol Germany GmbH*. The blue bars show the relative amount of the respective linear (*n*-) alkanes while the yellow bars the amount of the respective branched (*iso*-) alkanes. According to the spectrum the wax contains 71.3% of *n*-alkanes and 28.7% of *iso*-alkanes. The average number of C-atoms amounts to 30.5.

This information is available free of charge via the Internet at http://pubs.acs.org/.

AUTHOR INFORMATION

Corresponding Author

*E-mail: Thomas.sottmann@ipc.uni-stuttgart.de; Tel.: +49 711 685 64494; Fax: +49 711 685 64443.

ORCID:

Thomas Sottmann: 0000-0003-3679-3703

ACKNOWLEDGMENT

The authors thank the companies SASOL for providing the technical-grade oil SASOL*WAX 5805* and the respective GC-spectrum as well as Clariant for providing the technical grade surfactants of the *Genapol*® series. Also, we acknowledge the support of the Institut Laue Langevin (ILL) in Grenoble (France) and the Jülich Centre for Neutron Science *JCNS* at the Heinz Maier-Leibnitz Zentrum (MLZ) in providing the facilities for the SANS measurements.

We furthermore want to thank the SANS Teams consisting of S. Dieterich, J. Fischer, S. Lülsdorf, S.-Y. Tseng, O. Wrede and D. Zauser for their help during the SANS measurements. K.S. and T.S. acknowledge the German Research Foundation (DFG) for the funding within the Collaborative Research Center (CRC 1333).

REFERENCES

(1) Strey, R. Microemulsion microstructure and interfacial curvature. *Colloid Polym. Sci.* **1994**, *272*, 1005–1019.

(2) Sottmann, T.; Strey, R.; Lyklema, J. (eds.). *Microemulsion*. In: Fundamentals of Interface and Colloid Science, 1st ed. 5; Academic Press: London, San Diego, **2005**, 5.1–5.96.

(3) Kahlweit, M.; Strey, R. Phase Behavior of Ternary Systems of the Type H_2O–Oil–Nonionic Amphiphile (Microemulsions). *Angew. Chem. Int. Ed. Engl.* **1985**, *24*, 654–668.

(4) Schubert, K.-V.; Strey, R.; Kline, S. R.; Kaler, E. W. Small angle neutron scattering near Lifshitz lines: Transition from weakly structured mixtures to microemulsions. *J. Chem. Phys.* **1994**, *101*, 5343–5355.

(5) Danielsson, I.; Lindman, B. The definition of microemulsion. *Colloids Surf.* **1981**, *3*, 391–392.

(6) Hoar, T. P.; Schulman, J. H. Transparent Water-in-Oil Dispersions: The Oleopathic Hydro-Micelle. *Nature* **1943**, *152*, 102-103.

(7) Schulman, J. H.; Prince, L. M. Mechanism of Formation and Structure of Micro Emulsions by Electron Microscopy. *J. Phys. Chem.* **1959**, *63*, 1677–1680.

(8) Kahlweit, M.; Strey, R.; Haase, D.; Firman, P. Properties of the Three-Phase Bodies in H_2O–Oil–Nonionic Amphiphile Mixtures. *Langmuir* **1988**, *4*, 785–790.

(9) Kahlweit, M.; Strey, R. Phase Behavior of Quinary Mixtures of the Type H_2O–oil–Nonionic Amphiphile–Ionic Amphiphile–Salt. *J. Phys. Chem.* **1988**, *92*, 1557–1563.

(10) Penders, M. H. G. M.; Strey, R. Phase Behavior of the Quaternary System H_2O/*n*-Octane/C_5E_5/*n*-Octanol: Role of the Alcohol in Microemulsions. *J. Phys. Chem.* **1995**, *99*, 10313–10318.

(11) Lekkerkerker, H. N. W.; Kegel, W. K.; Overbeek, J. T. G. Phase Behavior of Ionic Microemulsions. *Ber. Bunsenges. Phys. Chem.* **1996**, *100*, 206–217.

(12) Schubert, K.-V.; Kaler, E. W. Nonionic Microemulsions. *Ber. Bunsenges. Phys. Chem.* **1996**, *100*, 190–205.

(13) Shinoda, K. *Solvent Properties of Surfactant Solutions*, 2nd ed.; Surfactant science series; Marcel Dekker, Inc.: New York, NY, 1967.

(14) Bellocq, A.-M.; Biais, J.; Clin, B.; Gelot, A.; Lalanne, P.; Lemanceau, B. Three—dimensional phase diagram of the brine-toluene-butanol-sodium dodecyl sulfate system. *J. Colloid Interface Sci.* **1980**, *74*, 311–321.

(15) Eicke, H. F.; Robb, I. D. (eds.). *The Microemulsion Concept in Nonpolar Surfactant Solutions*. In: Microemulsions; Springer US: Boston, MA, **1982**.

(16) Langevin, D. Microemulsions and Liquid Crystals. *Mol. Cryst. Liq. Cryst.* **1986**, *138*, 259–305.

(17) Sottmann, T.; Strey, R. Ultralow interfacial tensions in water–*n*-alkane–surfactant systems. *J. Chem. Phys.* **1997**, *106*, 8606–8615.

(18) Shinoda, K.; Friberg, S. Microemulsions: Colloidal aspects. *Adv. Colloid Interface Sci.* **1975**, *4*, 281–300.

(19) Schechter, R. S.; Wade, W. H.; Weerasooriya, U.; Weerasooriya, V.; Yiv, S. Synthesis and Performance of Isomer-free Secondary Alkane Sulfonate Surfactants. *J. Dispersion Sci. Technol.* **1985**, *6*, 223–235.

(20) Langevin, D.; Chen, S.-H. (eds.). *Low Interfacial Tensions in Microemulsion Systems*. In: Structure and Dynamics of Strongly Interacting Colloids and Supramolecular Aggregates in Solution; Springer Netherlands: Dordrecht, **1992**, 325–349.

(21) Wade, W. H.; Morgan, J. C.; Schechter, R. S.; Jacobson, J. K.; Salager, J. L. Interfacial Tension and Phase Behavior of Surfactant Systems. *Soc. Petrol. Eng. J.* **2013**, *18*, 242–252.

(22) Aveyard, R.; Binks, B. P.; Clark, S.; Mead, J. Interfacial tension minima in oil–water–surfactant systems. Behavior of alkane–aqueous NaCl systems containing aerosol OT. *J. Chem. Soc., Faraday Trans. 1* **1986**, *82*, 125–142.

(23) Olsson, U.; Shinoda, K.; and Lindman, B.; Olsson, U.; Shinoda, K.; Lindman, B. Change of the Structure of Microemulsions with the Hydrophile-Lipophile Balance of Nonionic Surfactant As Revealed by NMR Self-Diffusion Studies. *J. Phys. Chem.* **1986**, *90*, 4083–4088.

(24) Schwuger, M.-J.; Stickdorn, K.; Schomaecker, R. Microemulsions in Technical Processes. *Chem. Rev.* **1995**, *95*, 849–864.

(25) Stubenrauch, C. *Microemulsions: Background, new concepts, applications, perspectives*; Wiley: Chichester West Sussex U.K., Ames Iowa, **2009**.

(26) Kumar, A.; Kushwaha, V.; Sharma, P. K. Pharmaceutical Microemulsion: Formulation, Characterization and Drug deliveries across skin. *Int. J. Drug Dev. & Res.* **2014**, *6*, 1–21.

(27) Schambil, F.; Schwuger, M. J. CPS LG 315 Correlation between the phase behavior of ternary systems and removal of oil in the washing process. *Colloid Polym. Sci.* **1987**, *265*, 1009–1017.

(28) Kling, W.; Lange, H. Theory of the washing process. *J. Am. Oil Chem. Soc.* **1960**, *37*, 30–32.

(29) Donaldson, E. C.; Chilingar, G. V.; Yen, Teh Fu (eds). Vol 17B. *Enhanced oil recovery II*; In Series: Developments in petroleum science; Elsevier: Amsterdam, New York, **1989**.

(30) Nazar, M. F.; Shah, S. S.; Khosa, M. A. Microemulsions in Enhanced Oil Recovery: A Review. *Pet. Sci. Technol.* **2011**, *29*, 1353–1365.

(31) Sharma, M. K.; Shah, D. O. *Macro- and Microemulsions in Enhanced Oil Recovery: In: Macro- and Microemulsions*; ACS Symposium Series 272; American Chemical Society: Washington, D.C., **1985**.

(32) Shah, D. O.; Schechter, R. S. *Improved Oil Recovery by Surfactant and Polymer Flooding*; Academic Press; Elsevier: New York, **1977**.

(33) Schomaecker, R.; Robinson, B. H.; Fletcher, P. D. I. Interaction of Enzymes with Surfactants in Aqueous Solution and in Water-in-oil Microemulsions. *J. Chem. Soc., Faraday Trans. 1* **1988**, *84*, 4203–4212.

(34) Schmidt, J.; Guesdon, C.; Schomäcker, R. Engineering Aspects of Preparation of Nanocrystalline Particles in Microemulsions. *J. Nanopart. Res.* **1999**, *1*, 267–276.

(35) Müller, M.; Kasaka, Y.; Müller, D.; Schomäcker, R.; Wozny, G. Process Design for the Separation of Three Liquid Phases for a Continuous Hydroformylation Process in a Miniplant Scale. *Ind. Eng. Chem. Res.* **2013**, *52*, 7259–7264.

(36) Volovych, I.; Neumann, M.; Schmidt, M.; Buchner, G.; Yang, J.-Y.; Wölk, J.; Sottmann, T.; Strey, R.; Schomäcker, R.; Schwarze, M. A novel process concept for the three step Boscalid® synthesis. *RSC Adv.* **2016**, *6*, 58279–58287.

(37) Web of Science. *Publications of R. Schomäcker and its citations* (accessed September 30, 2018).

(38) Miller, C. A.; Raney, K. H. Solubilization—emulsification mechanisms of detergency. *Colloids and Surfaces A: Physicochemical and Engineering Aspects* **1993**, *74*, 169–215.

(39) Bera, A.; Mandal, A. Microemulsions: A novel approach to enhanced oil recovery: a review. *J. Petrol. Explor. Prod. Technol.* **2015**, *5*, 255–268.

(40) Sottmann, T.; Lade, M.; Stolz, M.; Schomäcker, R. Phase behavior of non-ionic microemulsions prepared from technical-grade surfactants. *Tenside, Surfactants, Deterg.* **2002**, *39*, 20–28.

(41) Ryan, L. D.; Schubert, K.-V.; Kaler, E. W. Phase Behavior of Microemulsions Made with *n*-Alkyl Monoglucosides and *n*-Alkyl Polyglycol Ethers. *Langmuir* **1997**, *13*, 1510–1518.

(42) Burauer, S.; Sottmann, T.; Strey, R. Nonionic microemulsions with cyclic oils: Oil penetration, efficiency and monomeric solubility. *Tenside, Surfactants, Deterg.* **2000**, *37*, 8–16.

(43) Lade, O.; Beizai, K.; Sottmann, T.; Strey, R. Polymerizable Nonionic Microemulsions: Phase Behavior of H_2O– *n*-Alkyl Methacrylate– *n*-Alkyl Poly(ethylene glycol) Ether (C_iE_j). *Langmuir* **2000**, *16*, 4122–4130.

(44) Engelskirchen, S.; Elsner, N.; Sottmann, T.; Strey, R. Triacylglycerol microemulsions stabilized by alkyl ethoxylate surfactants-A basic study. Phase behavior, interfacial tension and microstructure. *J. Colloid Interface Sci.* **2007**, *312*, 114–121.

(45) Wormuth, K. R.; Kaler, E. W. Microemulsifying Polar Oils. *J. Phys. Chem.* **1989**, *93*, 4855–4861.

(46) Queste, S.; Salager, J. L.; Strey, R.; Aubry, J. M. The EACN scale for oil classification revisited thanks to fish diagrams. *J. Colloid Interface Sci.* **2007**, *312*, 98–107.

(47) Kahlweit, M.; Strey, R.; Busse, G. Microemulsions: A Qualitative Thermodynamic Approach. *J. Phys. Chem.* **1990**, *94*, 3881–3894.

(48) Sottmann, T.; Strey, R. Shape Similarities of Ultra-Low Interfacial Tension Curves in Ternary Microemulsion Systems of the Water-Alkane-C_iE_j Type. *Ber. Bunsenges. Phys. Chem.* **1996**, *100*, 237–241.

(49) Teubner, M.; Strey, R. Origin of the scattering peak in microemulsions. *J. Chem. Phys.* **1987**, *87*, 3195–3200.

(50) Pieruschka, P.; Safran, S. A.; Marčelja, S. T. Comment on ''Fluctuating interfaces in microemulsion and sponge phases''. *Phys. Rev. E* **1995**, *52*, 1245–1247.

(51) Strey, R.; Sottmann, T. Evidence of corresponding states in ternary microemulsions of water - alkane - C_iE_j. *J. Phys.: Condens. Matter* **1996**, *8*, A39-A48.

(52) Sottmann, T.; Strey, R.; Chen, S.-H. A small-angle neutron scattering study of nonionic surfactant molecules at the water–oil interface: Area per molecule, microemulsion domain size, and rigidity. *J. Chem. Phys.* **1997**, *106*, 6483–6491.

(53) Frielinghaus, H.; Feoktystov, A.; Berts, I.; Mangiapia, G. KWS-1: Small-angle scattering diffractometer. *JLSRF* **2015**, *1*, 1–4.

(54) Foster, T.; Sottmann, T.; Schweins, R.; Strey, R. Small-angle neutron scattering from giant water-in-oil microemulsion droplets. I. Ternary system. *J. Chem. Phys.* **2008**, *128*, 54502.

(55) Schubert, K.-V.; Strey, R. Small-angle neutron scattering from microemulsions near the disorder line in water/formamide–octane-C_iE_j systems. *J. Chem. Phys.* **1991**, *95*, 8532–8545.

(56) Burauer, S.; Sachert, T.; Sottmann, T.; Strey, R. On microemulsion phase behavior and the monomeric solubility of surfactant. *Phys. Chem. Chem. Phys.* **1999**, *1*, 4299–4306.

(57) Kahlweit, M.; Strey, R.; Rosano, H.L. (eds.) *In: Proceeding of Vth International Conference on Surface and Colloid Science, Potsdam, New York,* **1985**.

(58) Jahn, W.; Strey, R., Meunier, J. et al. (eds.). Images of Bicontinuous Microemulsions by Freeze Fracture Electron Microscopy. *In: Physics of Amphiphilic Layers. Springer Proceedings in Physics, Springer* **1987**, *21*, 353–356.

(59) Davis, H. T.; Bodet, J. F.; Scriven, L. E.; Miller, W. G. Microstructure and transport in midrange microemulsions. *Physica A* **1989**, *157*, 470–481.

(60) Lindman, B.; Meunier, J. et al. (eds.). Molecular Self-Diffusion and Microemulsion Bicontinuity. *In: Physics of Amphiphilic Layers. Springer Proceedings in Physics, Springer* **1987**, *21*, 357–363.

(61) Helfrich, W. Elastic Properties of Lipid Bilayers: Theory and Possible Experiments. *Z. Naturforsch., C: J. Biosci.* **1973**, *28*, 693–703.

(62) Morse, D. C. Topological instabilities and phase behavior of fluid membranes. *Phys. Rev. E* **1994**, *50*, R2423-R2426.

(63) Pieruschka, P.; Safran, S. A. Random Interface Model of Sponge Phases. *Europhys. Lett.* **1995**, *31*, 207–212.

(64) Golubović, L. Passages and droplets in lamellar fluid membrane phases. *Phys. Rev. E* **1994**, *50*, R2419-R2422.

(65) Gompper, G.; Kroll, D. M. Membranes with Fluctuating Topology: Monte Carlo Simulations. *Phys. Rev. Lett.* **1998**, *81*, 2284–2287.

(66) Strey, R.; Winkler, J.; Magid, L. Small-Angle Neutron Scattering from Diffuse Interfaces. 1. Mono- and Bilayers in the Water–Octane–$C_{12}E_5$ system. *J. Phys. Chem.* **1991**, *95*, 7502–7507.

(67) Porod, G.; Glatter, O.; Kratky, O. *Small angle X-ray scattering*, 2nd printing; Academic Press: London, **1983**.

(68) Lichterfeld, F.; Schmeling, T.; Strey, R. Microstructure of Microemulsions of the System H_2O–*n*-Tetradecane–$C_{12}E_5$. *J. Phys. Chem.* **1986**, *90*, 5762–5766.

(69) Mittal, K. L.; Kumar, P., (Eds.). *Handbook of Microemulsion Science and Technology*; Marcel Dekker; CRC Press; Taylor & Francis Group: New York, NY, **1999**.

FIGURES

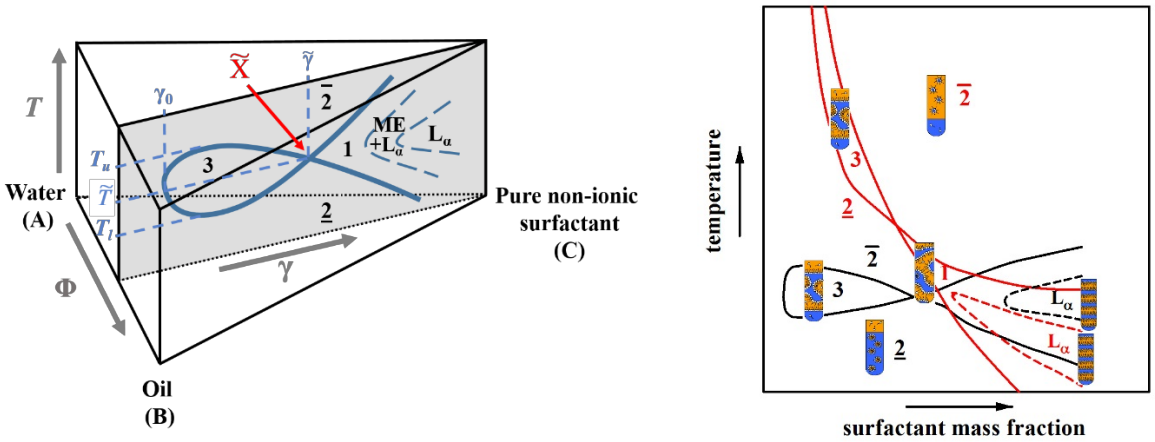

Figure 1. Left: Schematic representation of the Gibbs phase prism to illustrate the phase behavior of ternary systems of the type water (A) – oil (B) – pure nonionic surfactant (C) as function of composition and temperature. The *T*(γ)-section, also referred to as "fish"-diagram, conducted at a constant volume fraction ☐ of oil in the water/oil mixture is highlighted in grey. Right: Schematic representation of the *T*(γ)-section recorded for a microemulsion stabilized with

a pure (black line) and technical-grade surfactant (red line). While a horizontal three-phase body is found for the former system, a strongly distorted three-phase body is found for the latter system, as a consequence of the fact that the hydrophobic homologues are extracted from the amphiphilic film into oil-rich domains and excess phase.

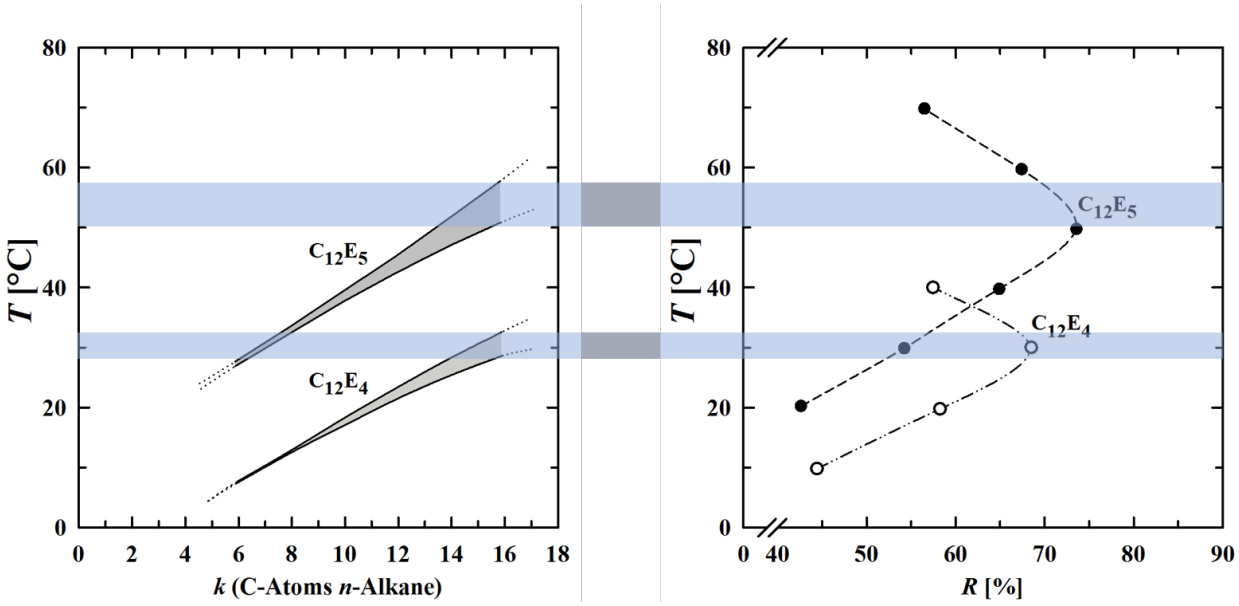

Figure 2. Left: Temperature interval (T_u-T_l) of the three-phase body for the systems water – *n*-alkane (C_kH_{2k+2}) – $C_{12}E_4$ and $C_{12}E_5$ versus the chain length of the *n*-alkanes *k*. Right: Results of washing tests performed on *n*-hexadecane contaminated fabrics using aqueous solutions of the two pure surfactants $C_{12}E_4$ and $C_{12}E_5$. The washing temperature is plotted versus the washing efficiencies *R* obtained from photometric measurements. As shown, the maximum oil removal is achieved at the temperature of the three-phase interval of the respective water – *n*-hexadecane – $C_{12}E_4$ and $C_{12}E_5$ system. (Reproduced from[27] with permission from *Springer Nature*.)

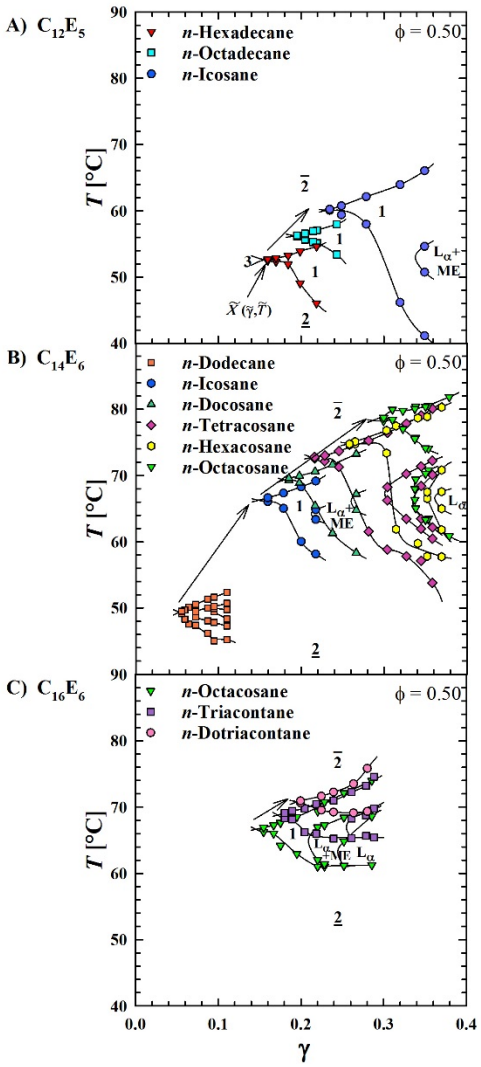

Figure 3. $T(\gamma)$-sections of various ternary microemulsion systems of the type water **–** *n*-alkane – pure C_iE_j surfactant adjusting a constant volume fraction of oil in the mixture of oil and water of $\square = 0.50$. The influence of the *n*-alkane chain length *k* is studied using: A) the surfactant $C_{12}E_5$ to solubilize *n*-hexadecane ($C_{16}H_{34}$), *n*-octadecane ($C_{18}H_{38}$) and *n*-icosane ($C_{20}H_{42}$); B) the surfactant $C_{14}E_6$ to solubilize *n*-dodecane ($C_{12}H_{26}$), *n*-icosane, *n*-docosane ($C_{22}H_{46}$), *n*-tetracosane ($C_{24}H_{50}$), *n*-hexacosane ($C_{26}H_{54}$) and *n*-octacosane ($C_{28}H_{58}$); C) the surfactant $C_{16}E_6$ to solubilize *n*-octacosane, *n*-triacontane ($C_{30}H_{62}$) and *n*-dotriacontane ($C_{32}H_{66}$). Note that an increase of *k* leads to a shift of the phase boundaries to higher temperatures. At the same time the respective surfactant becomes less efficient.

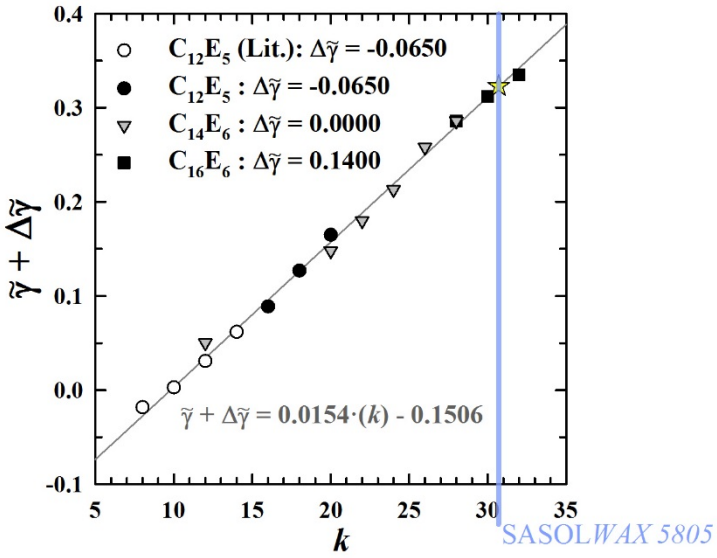

Figure 4. Dependence of the "adapted" surfactant mass fraction $\tilde{\gamma} + \Delta\tilde{\gamma}$ at the $\tilde{X}$-point as a function of the oil chain length k of the *n*-alkanes for ternary systems of the type H_2O – *n*-alkane – C_iE_j at $\square = 0.50$. In order to compare the $\tilde{\gamma}$-values of different surfactant systems, the values of the $C_{12}E_5$-systems are shifted by $\Delta\tilde{\gamma}[C_{12}E_5] = -0.0650$, while the values of the $C_{16}E_6$-systems are altered by $\Delta\tilde{\gamma}[C_{16}E_6] = 0.1400$. Furthermore, the $\tilde{\gamma} + \Delta\tilde{\gamma}$ value (asterisk) of the ternary system H_2O – SASOL*WAX 5805* – $C_{16}E_6$ (see next section) is added, yielding an equivalent alkane carbon number EACN (SASOL*WAX 5805*) ≈ 30.8. Note that the values for the $C_{12}E_5$-systems containing the *n*-alkanes *n*-octane to *n*-tetradecane are reproduced from Ref. 56 with permission from the *PCCP Owner Societies*.

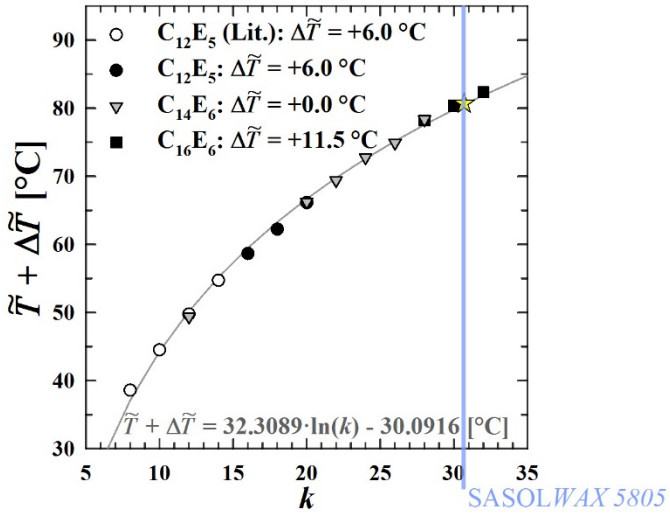

Figure 5. Dependence of the "adapted" phase inversion temperature $\tilde{T} + \Delta\tilde{T}$ as a function of the oil chain length *k* of the *n*-alkanes for ternary systems of the type H_2O – *n*-alkane – C_iE_j at ☐ = 0.50. In order to compare the $\tilde{T}$ values of different surfactant systems, the values of the $C_{12}E_5$-systems are shifted by $\Delta\tilde{T}[C_{12}E_5] = 6.0$ K, while the values of the $C_{16}E_6$-systems are altered by $\Delta\tilde{T}[C_{16}E_6] = 11.5$ K. Furthermore, the $\tilde{T} + \Delta\tilde{T}$ value (asterisk) of the ternary system H_2O – SASOL*WAX 5805* – $C_{16}E_6$ (see next section) is added, yielding an equivalent alkane carbon number EACN (SASOL*WAX 5805*) ≈ 30.8. Note that the values for the $C_{12}E_5$-systems containing the *n*-alkanes *n*-octane to *n*-tetradecane are reproduced from Ref. 56 with permission from the *PCCP Owner Societies*.

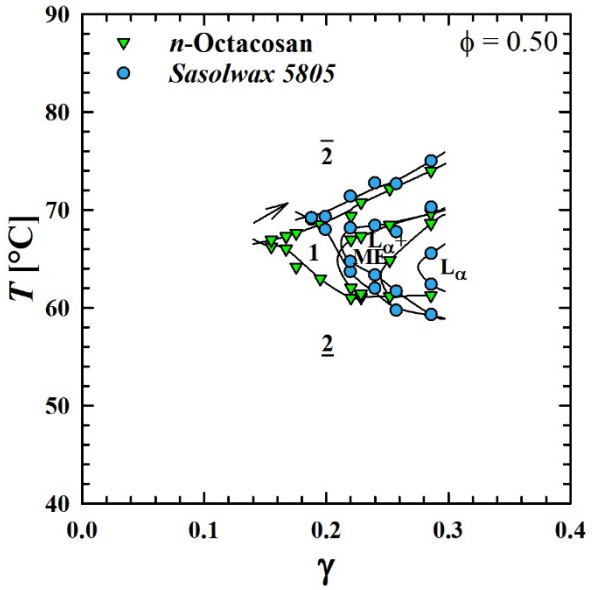

Figure 6. *T*(γ)-sections of the system H_2O – SASOL*WAX 5805* – $C_{16}E_6$ in comparison to the system water – *n*-octacosane – $C_{16}E_6$. Both *T*(γ)-sections are recorded at □ = 0.50. As shown, the SASOL*WAX 5805* can be solubilized in form of a microemulsion. Comparing the phase diagrams, the phase boundaries of the SASOL*WAX 5805*-containing system are shifted to slightly higher temperatures and higher γ-values.

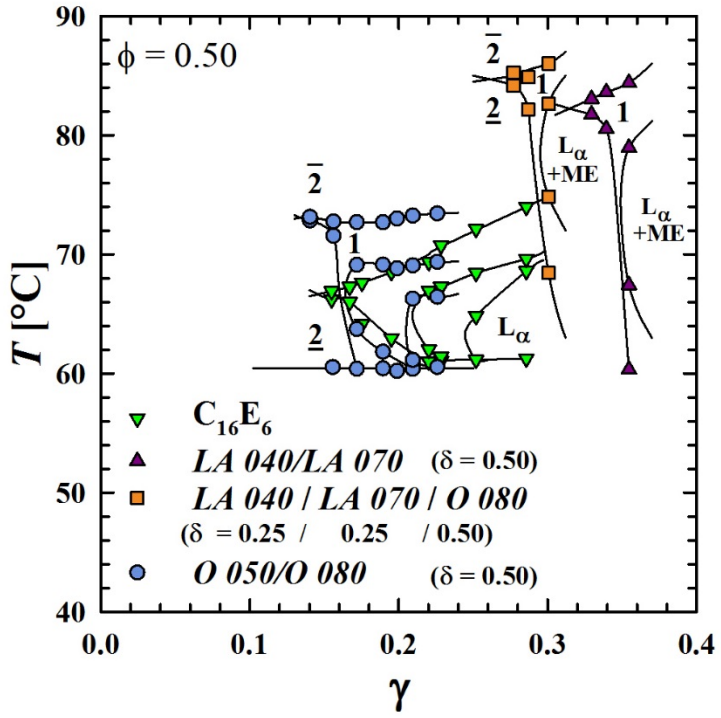

Figure 7. $T(\gamma)$-sections (recorded at $\square = 0.50$) of the systems water – *n*-octacosane – Genapol®, which are technical-grade alcohol ethoxylates (C_iE_j) in comparison to the system water – *n*-octacosane – $C_{16}E_6$. Three different mixtures of technical-grade Genapol® surfactants are used. Starting with the mixture *Genapol LA 040/ Genapol LA 070* ($\delta = 0.50$), 50 wt% of the *LA 040/LA 070* mixture is replaced with the more efficient and hydrophobic *Genapol O 080* ($\delta = 0.25, 0.25, 0.50$). The most efficient solubilization of *n*-octacosane in water is obtained using a mixture of *Genapol O 050/ Genapol O 080* ($\delta = 0.50$).

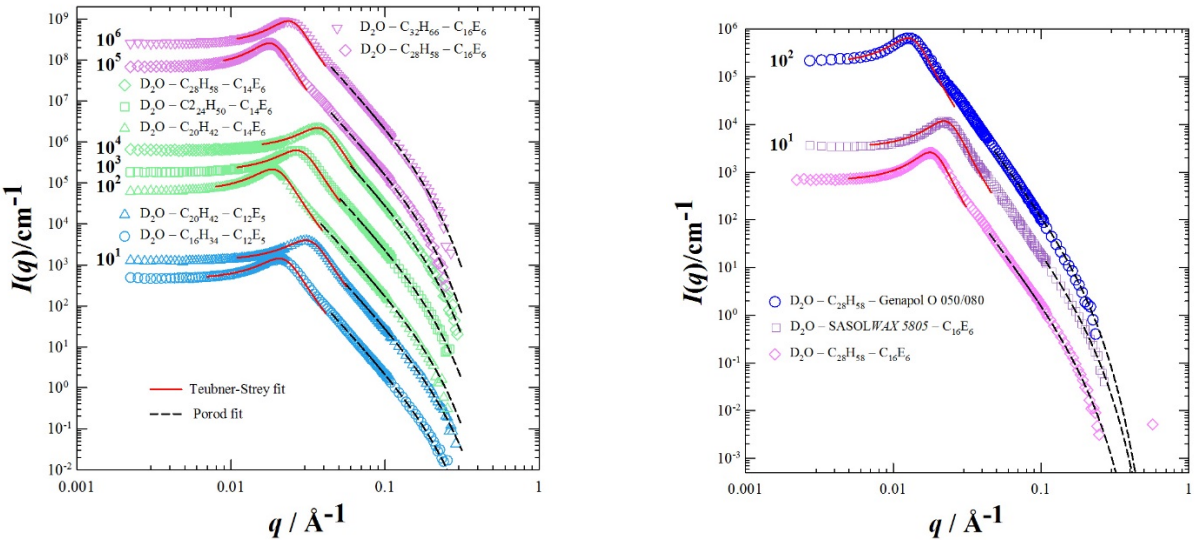

Figure 8. SANS scattering curves of symmetric microemulsions recorded near the respective $\widetilde{X}$-point at a surfactant mass fraction of the order of $\gamma \approx \tilde{\gamma}$ +0.01 and $\square = 0.50$. Left: Ternary systems of the type D_2O – *n*-alkane – C_iE_j after subtraction of the incoherent background increasing the alkyl chain length *k* of the *n*-alkanes from *n*-hexadecane ($C_{16}H_{34}$) to *n*-dotriacontane ($C_{32}H_{66}$). The measurements are conducted for the three pure surfactants $C_{12}E_5$ (blue symbols), $C_{14}E_6$ (green symbols) and $C_{16}E_6$ (pink symbols). Right: SANS-curves of D_2O – *n*-octacosane – *Genapol O 050/080* and D_2O – SASOL*WAX 5805* – $C_{16}E_6$ as well as D_2O – *n*-octacosane – $C_{16}E_6$ shown for comparison. The solid lines are the fits of the scattering peaks by the *Teubner-Strey* model[49]. The higher *q*-part of the scattering curve is described by the *Porod* model for diffuse interfaces[66,67] (dashed lines).

TABLES

Table 1. $\tilde{X}$-points, $\tilde{\gamma}$, $\tilde{T}$ (*PIT*) and α-values of all studied ternary systems of the type H_2O – oil – C_iE_j at □ = 0.50. $\tilde{\gamma}$ and $\tilde{T}$ are determined with a precision of ± 0.005 and ± 0.5 K, respectively. Using a mixture of two surfactants, the mass fraction of co-surfactants in the surfactant mixture is given by δ_{CiEj}, i.e. for the *Genapol LA 040/ Genapol LA 070/ Genapol O 080* mixture $\delta_{LA040} = 0.25$, $\delta_{LA070} = 0.25$ and $\delta_{O080} = 0.50$.

System components	δ	$\tilde{\gamma}$	$\tilde{T}$/ °C	α
H_2O – *n*-hexadecane – $C_{12}E_5$	0.000	0.154	52.7	0.436
H_2O – *n*-octadecane – $C_{12}E_5$	0.000	0.192	56.2	0.437
H_2O – *n*-icosane – $C_{12}E_5$	0.000	0.230	60.2	0.441
H_2O – *n*-dodecane – $C_{12}E_5$	0.000	0.050	49.4	0.430
H_2O – *n*-icosane – $C_{14}E_6$	0.000	0.148	66.3	0.441
H_2O – *n*-docosane – $C_{14}E_6$	0.000	0.180	69.4	0.438
H_2O – *n*-tetracosane – $C_{14}E_6$	0.000	0.213	72.8	0.445
H_2O – *n*-hexacosane – $C_{14}E_6$	0.000	0.258	74.9	0.437
H_2O – *n*-octacosane – $C_{14}E_6$	0.000	0.286	78.3	0.447
H_2O – *n*-octacosane – $C_{16}E_6$	0.000	0.146	66.7	0.447
H_2O – *n*-triacontane – $C_{16}E_6$	0.000	0.172	68.9	0.448
H_2O – *n*-dotriacontane – $C_{16}E_6$	0.000	0.195	70.9	0.449
H_2O – SASOL*WAX 5805* – $C_{16}E_6$	0.000	0.183	69.2	0.478
H_2O – *n*-octacosane – *Genapol LA 040/ Genapol LA 070*	0.500	0.316	82.2	0.447
H_2O – *n*-octacosane – *Genapol LA 040/ Genapol LA 070/ Genapol O 080*	0.25/0.25/0.50	0.261	84.8	0.447
H_2O – *n*-octacosane – *Genapol O 050/ Genapol O 080*	0.500	0.134	73.3	0.446

Table 2. Temperature, surfactant mass γ and volume fraction Φ_c of the (symmetric) pure and technical-grade components containing microemulsion samples of the type D_2O – *n*-alkane (C_kH_{2k+2}) – C_iE_j studied via SANS. Given are the domain size d_{TS}, correlation length ξ_{TS} and amphiphilicity factor f_a obtained from the *Teubner-Strey*-analysis[49] together with the volume fraction of surfactant in the interface $\Phi_{c,i}$, the diffuseness of the amphiphilic film *t*, the total specific internal interface *S*/*V* and the volume fraction of surfactant molecules solubilized within the oil-phase of the microemulsion $\Phi_{mon,b}$ yielded by the analysis of the large *q*-part of the scattering curve using the *Porod* decay for diffuse interfaces[66,67]. According to *Safran et al.*[63] the renormalized bending rigidity κ_{SANS} can be obtained from d_{TS} and ξ_{TS}. The measurements are performed at constant Φ = 0.50 near the $\widetilde{X}$-point of the respective system.[a]

i	*j*	*k*	*T*/ °C	Φ_c	ξ_{TS}/ Å	d_{TS}/ Å	f_a	κ_{SANS}/k_BT	*S*/*V*/ Å^{-1}	*t*/ Å	$\Phi_{c,i,}$	$\Phi_{mon,b}$
12	5	16	49.8	0.153	154	292	-0.832	0.447	0.012	5.5	0.134	0.04
12	5	20	57,2	0.226	102	196	-0.829	0.443	0.018	5.0	0.209	0.04
14	6	20	62,7	0.148	179	325	-0.845	0.467	0.011	5.5	0.136	0.03
14	6	24	68,7	0.210	120	226	-0.836	0.453	0.016	5.5	0.197	0.03
14	6	28	74.9	0.280	87.3	165	-0.835	0,451	0.022	5.5	0.271	0.03
16	6	28	64,6	0.148	203	342.	-0.866	0,505	0.011	6.0	0.139	0.02
16	6	32	70.8	0.195	147	257	-0.856	0.486	0.014	6.0	0.184	0.03
16	6	30.5*	66.6	0.193	155	274	-0.854	0.482	0.014	5.5	0.184	0.02
18	6.5*	28	67.8	0.135	263	478	-0.846	0.468	0.009	6.0	0.124	0.03

[a] Note that for the technical surfactant *Genapol O 0j0* the scattering length densities ϱ of its pure counterparts, namely $C_{18}E_5$ and $C_{18}E_8$, were used. * Average chain length of the SASOL*WAX 5805* and the technical surfactants *Genapol O 0j0*.

For Table of Contents only

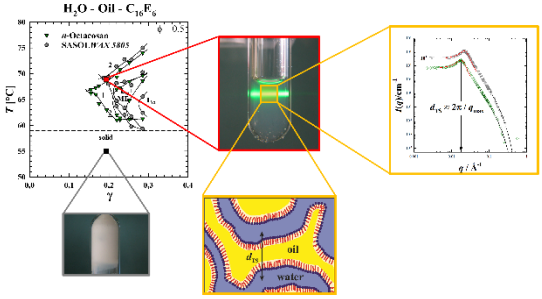

SUPPORTING INFORMATION

Phase behavior and microstructure of symmetric nonionic microemulsions with long-chain *n*-alkanes and waxes

*Kristina Schneider[a], Tim M. Ott[a], Ralf Schweins[b], Henrich Frielinghaus[c], Oliver Lade[d], Thomas Sottmann[a]**

[a]Institut für Physikalische Chemie, Universität Stuttgart, Pfaffenwaldring 55, 70569 Stuttgart, Germany

[b]Institut Laue-Langevin, 71 avenue des Martyrs, CS 20156, 38042 GRENOBLE Cedex 9, France

[c]Jülich Centre for Neutron Science JCNS at Heinz Maier-Leibnitz Zentrum (MLZ), Lichtenbergstraße 1, 85748 Garching, Germany

[d]Clariant Produkte (Deutschland) GmbH, G 860, Industriepark Höchst, August-Laubenheimer Straße 1, 65929 Frankfurt am Main, Germany

CORRESPONDING AUTHOR

Thomas Sottmann*, E-mail: thomas.sottmann@ipc.uni-stuttgart.de

Number of pages: 3
Number of tables: 1
Number of figures: 1

Table of Contents

Table S1. Macroscopic densities ϱ^0 and scattering length densities ϱ of the components of the investigated ternary microemulsion samples at T= 20°C. [a]

Figure S1. Distribution of linear and branched alkanes as a function of their number of C-atoms obtained from a gas chromatography (GC) spectrum of the SASOL*WAX 5805* recorded by the *Sasol Germany GmbH*. The blue bars show the relative amount of the respective linear (*n*-) alkanes while the yellow bars show the amount of the respective branched (*iso*-) alkanes. According to the spectrum the wax contains 71.3% of *n*-alkanes and 28.7% of *iso*-alkanes. The average number of C-atoms amounts to 30.5.

Table S1. Macroscopic densities ϱ^0 and scattering length densities ϱ of the components of the investigated ternary microemulsion samples at T= 20°C. [a]

Component	ϱ^0 (g/cm^3)	ϱ (10^{-6} Å^{-1})
Double-distilled H_2O	0.998	-0.560
D_2O	1.107	6.375
n-dodecane	0.748	-0.462
n-hexadecane	0.773	-0.428
n-octadecane	0.777	-0.413
n-icosane	0.789	-0.406
n-docosane	0.794	-0.397
n-tetracosane	0.799	-0.390
n-hexacosane	0.803	-0.374
n-octacosane	0.807	-0.379
n-triacontane	0.810	-0.375
n-dotriacontane	0.812	-0.371
SASOL*WAX 5805*	0.918	-0.422

$C_{12}E_5$	0.963	0.129
$C_{14}E_6$	0.970	0.140
$C_{16}E_6$	0.962	0.112
Genapol LA 040	0.950	0.061
Genapol LA 070	0.970	0.189
Genapol O 050	0.960	0.136
Genapol O 080	0.960	0.223

[a] Note that for the technical surfactants *Genapol LA 0j0* and *Genapol O 0j0* the scattering length densities ϱ of their pure counterparts, namely $C_{13}E_4$, $C_{13}E_7$, $C_{18}E_5$ and $C_{18}E_8$, were used.

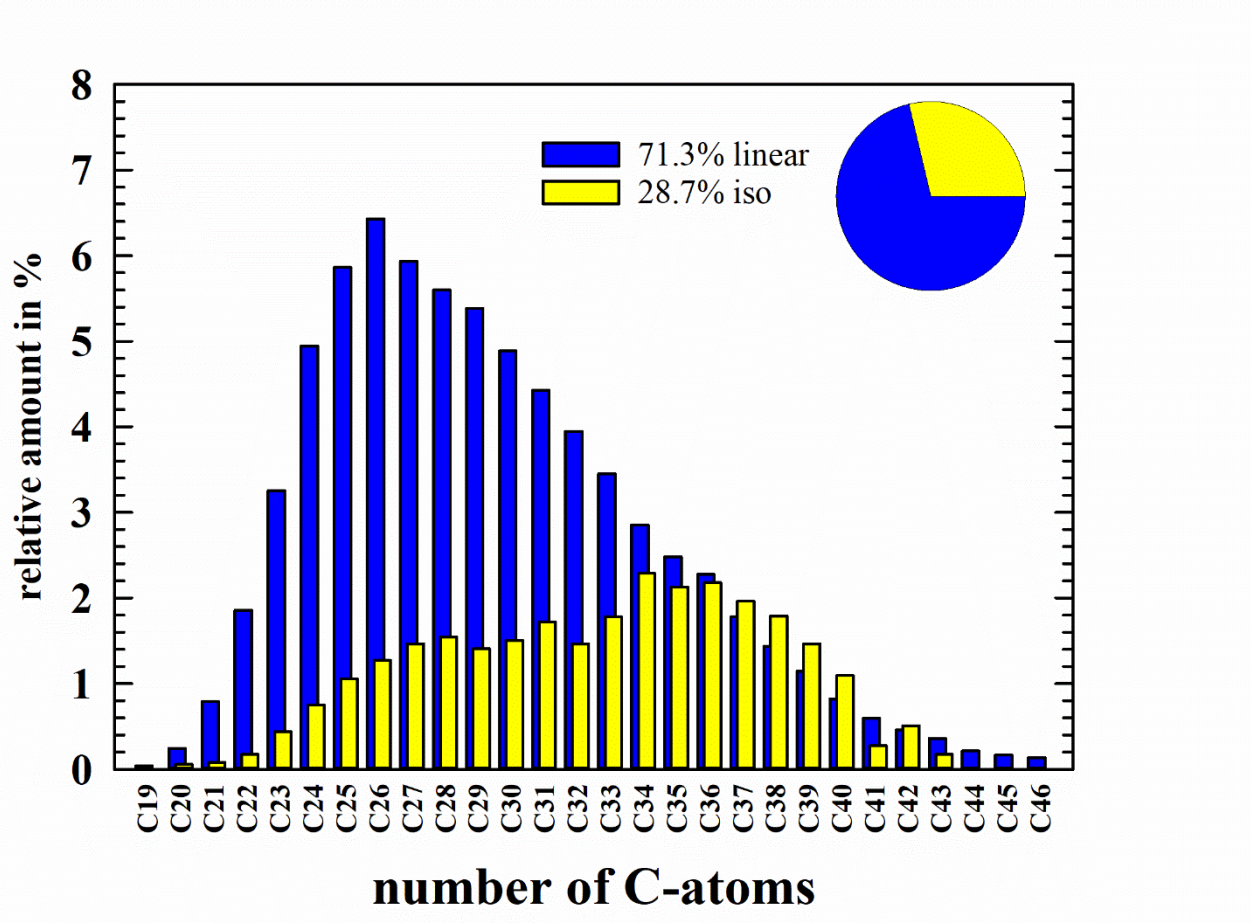

Figure S1. Distribution of linear and branched alkanes as a function of their number of C-atoms obtained from a gas chromatography (GC) spectrum of the SASOL*WAX 5805* recorded by the *Sasol Germany GmbH*. The blue bars show the relative amount of the respective linear (*n*-)

alkanes while the yellow bars show the amount of the respective branched (*iso*-) alkanes. According to the spectrum the wax contains 71.3% of *n*-alkanes and 28.7% of *iso*-alkanes. The average number of C-atoms amounts to 30.5.